SIMULATION-BASED CALCULATIONS OF THE PROTON DOSE IN PHASE CHANGE MEMORY CELLS

by

***Nevena S. ZDJELAREVIĆ*[1,2], *Ivan D. KNEŽEVIĆ*[1,2], *Miloš Lj. VUJISIĆ*[2] *and Ljubinko B. TIMOTIJEVIĆ*[2]**

[1]Public Company Nuclear Facilities of Serbia, Belgrade, Serbia
[2]Faculty of Electrical Engineering, University of Belgrade, Belgrade, Serbia

Scientific paper
DOI: 10.2298/NTRP1303299Z

Monte Carlo simulations of proton irradiation on phase change memory cells were conducted and the proton dose, in both the whole memory cell and in its active layer, calculated. The memory cell was modeled by a multi-layer stack consisting of two TiW electrodes and ZnS-SiO_2 films as insulators surrounding the active region. Materials considered for the active region were $Ge_2Sb_2Te_5$, $AgSbSe_2$, and $Si_2Sb_2Te_5$. The effects of exposing phase change memory cells to proton beams were investigated for various thicknesses of phase change materials and different proton energies. Radiation-induced changes in the investigated memory cells are presented, including the accumulation of atomic displacements and the thermal heating of the active region. Possible effects of these changes on cell operation are discussed.

Key words: phase change memory, phase change material, proton irradiation, Monte Carlo method, absorbed dose

INTRODUCTION

Phase change memory (PCM) is a term used to describe a class of non-volatile memory devices that exploit the unique behavior of phase change materials to store information. In 1968, electronic switching in amorphous chalcogenides was first observed, opening the way to applications in electronic storage [1]. The first PCM memory array was demonstrated in 1970 [2]. Recent progress has enabled the use of phase change alloys for practical high performance memory devices. Progress was made in the development of rapid crystallization alloys, as well as in the understanding of device properties. PCM is considered one of the most promising candidates for the next generation of non-volatile memories due to its good stability, high density and speed, simple cell structure, fast writing and reading ability, good endurance, non-volatility, and good compatibility with the complementary metal-oxide-semiconductor (CMOS) technology [3-5].

Every electronic device is subjected to radiation. In recent years, radiation effects on electronic devices have become a major concern for manufacturing companies. Nearly every chip is hit by some sort of radiation. The existence of intense regions of energetic proton radiation in space has stimulated considerable interest in the effects of proton radiation on semiconductor devices during the last several years. Energetic protons exist in the near-earth environment and are one of the most prominent sources of damage in electronic devices. They range in energy from tens of keV to hundreds of MeV, with fluxes as high as 10^5 protons/cm^{2}s for protons with energies higher than 30 MeV. Protons with these energies are able to easily penetrate shielding and impinge on electronics inside a spacecraft [6].

Since PCM could soon be applied in space industry and other radiation environments [7], it is important to explore their radiation tolerance and behavior.

Previous calculations of the proton dose and absorbed dose from ion beams in memory components mostly used, have nowadays shown that there are irradiation conditions and dose levels for every type of memory cell when radiation-induced changes of characteristics and functionality of these cells should be expected [8-10].

It has been a practice in previous years that irradiation simulations and calculations of the dose range where the radiation effects in a particular component structure are expected should be conducted before costly and time-consuming component irradiations at accelerating facilities. Moreover, irradiation experiments on memory chips can mask the information of the absorbed dose in the active layer of the memory

* Corresponding author; e-mail: nena_flo@hotmail.com

cell alone. This is because in this case, the radiation interacts not only with the memory cell, but with the whole memory chip whose peripheral circuits can be more radiation sensitive. Due to this fact, it is possible that problems may arise when these results have to be applied on the different structures or components containing the same active layer.

This paper presents the results of simulation-based calculations of the proton dose in PCM cells, as well as in their active layer, for a typical energy range and for different materials and thicknesses of the active layer.

OPERATION PRINCIPLES AND STRUCTURE OF A PCM CELL

The characteristics of phase change materials have been the subject of intense research over the last decade because of their unique properties [3-5]. There are various kinds of phase change materials. Most of them are chalcogenide compounds, including $Ge_2Sb_2Te_5$ (GST), $AgSbSe_2$ (ASS), and $Si_2Sb_2Te_5$ (SST), with GST being the most commonly used phase change material in PCM [11-16]. They have two stable physical states: amorphous and crystalline. In the amorphous state, the material is highly disordered and exhibits high resistivity. In the crystalline state, the material has a regular crystalline structure and exhibits low resistivity. Electrical resistivities of the crystalline and the amorphous phase differ by several orders of magnitude. PCM exploits this large resistivity difference between the two phases to store data [17].

The PCM has the ability to electrically induce the switching between amorphous and crystalline states by means of Joule heating produced by the current flow. Since both states are stable, no additional energy is required to store the data [18].

Typically, a cell in the amorphous state is regarded as a logic "0" (RESET state), and a cell in the crystalline state is regarded as a logic "1" (SET state). As fabricated, the phase change material is in the crystalline state because the processing temperature of the metal interconnect layers is sufficient to crystallize the phase change material. To RESET the PCM cell into the amorphous phase, the programming region is first melted and then rapidly quenched by applying a large electrical current pulse for a short time period. Doing so leaves a region of amorphous, highly resistive material in the cell. This amorphous region is in series with any crystalline region of the PCM and effectively determines the resistance of the PCM cell between the top and bottom electrode contacts. To SET the PCM cell into the crystalline phase, a lower amplitude current pulse is applied to anneal the programming region at a temperature above its crystallization temperature, but below its melting temperature over a period of time. To READ the state of the programming region, the resistance of the cell is measured by passing an electrical current small enough not to disturb its phase. Schematic pulse shapes are summarized in fig. 1. The time required for switching to the amorphous state is typically less than 100 ns, and the thermal time constant of the cell structure is typically only a few ns [14].

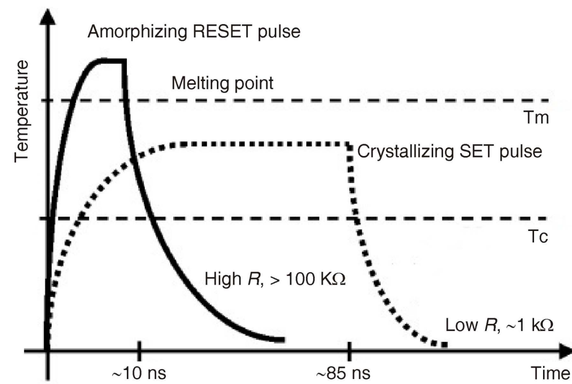

Figure 1. Electrical programming of a PCM cell, *i. e.* temperature in the programmed volume *vs.* time during SET and RESET programming pulses. T_c and T_m indicate the crystallization temperature and the melting point, respectively

Figure 2 shows the structure of a typical PCM cell. The phase change layer *(i. e.* active layer) is sandwiched between two TiW electrodes. These two TiW layers are isolated by $ZnS-SiO_2$ films. The thickness of the phase change layer is in the range from 50 nm to 200 nm [19].

Almost any material including metals, semiconductors, and insulators can exist in an amorphous phase and a crystalline phase. However, a very small subset of these materials simultaneously have all of the properties that make them useful for data storage technologies where the information is stored in the form of phase change material (*i. e.* large resistivity contrast between the crystalline and amorphous phase and the

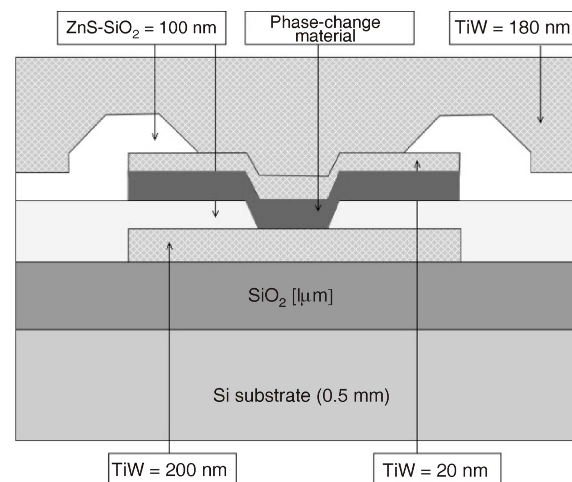

Figure 2. Structure of a typical PCM cell [19]

ability to be rapidly and repeatedly switched between these phases using electrical pulses). Three most commonly used materials (GST, ASS, and SST) were investigated as the PCM cell's phase change layer in simulations and calculations of the proton dose conducted in the present study.

SIMULATION AND CALCULATION METHODS

PCM cells are affected by three proton energy loss mechanisms: ionization, phononic excitations of the crystal lattice, and atomic displacement. All three modes of energy deposition are included in the calculated values of the absorbed dose [20].

When proton penetrates into the material, it first interacts with its electrons, both the single ones and collectively. The proton loses energy to material electrons in a process known as ionization. It loses energy to material electrons through ionization, thus increasing the concentration of free electrons or electron-hole pairs [20].

Towards the end of the proton's trajectory, ionization becomes less efficient and nuclear collisions begin to dominate. When the proton collides with a target nucleus, it imparts some recoil energy to its atom. If the transferred energy is larger than the threshold displacement energy, the incident proton will displace atoms in the material from their lattice sites. The resulting defects alter the electronic characteristics of the material. If the transferred energy is less than the threshold displacement energy, it is assumed that the atom returns to its lattice site and its energy is transferred into target phonons [20].

Simulations of protons passing through a PCM cell were performed using the Monte Carlo program called TRIM (TRansport of Ions in Mater) which is a part of the SRIM software suite. TRIM is based on the Monte Carlo simulation method, namely the binary collision approximation with a random selection of the impact parameter on the colliding ion. It calculates the stopping and range of ions into matter using the quantum mechanical treatment of ion-atom collisions. The ion and atom suffer a screened Coulomb collision including exchange and correlation interactions between the overlapping electron shells. The ion creates electron excitations and plasmons within the target by long-range interactions. The ion charge state within the target is described using the concept of the effective charge that includes a charge state that depends on velocity and long-range screening, due to the collective electron sea of the target. TRIM calculates all relevant kinetic phenomena associated with the proton's energy loss: ionization, atomic displacements, and phonon production [21].

The TRIM program has two main limitations: the first is that there is no build-up of ions or damage in the target, the second one is that the target temperature is considered to be 0 ºK. In spite of these limitations, several experiments have been reported at very low temperatures (15-40 K), validating the TRIM results [21]. Also, TRIM has been successfully used for simulations of radiation effects in various kinds of memory cells and components [8-10, 22].

The simulations were restricted to monoenergetic unidirectional beams, perpendicularly incident on the PCM cell surface. As a type of TRIM calculations, a *Detailed Calculation with Full Damage Cascades* has been chosen in the TRIM Setup Window in order to obtain the most detailed files on ion interactions.

In the setup, the Window target was defined with 6 different layers: 180 nm TiW (layer 1), 100 nm ZnS-SiO_2 (layer 2), 20 nm TiW (layer 3), a varying thickness phase change layer (layer 4), 100 nm ZnS-SiO_2 (layer 5), and 200 nm TiW (layer 6). TRIM divides the target material into 100 equal subunits (segments) and the program output files contain data for each of these segments regarding deposition energy in the material.

The densities given by TRIM for the constitutive compounds of the PCM cell were changed to more accurate values: 14.8 g/cm^3 for TiW, 3.65 g/cm^3 for ZnS-SiO_2, and 6.15 g/cm^3 for $Ge_2Sb_2Te_5$ [19].

Proton energy was varied across the low energy part (50-200 keV) of the typical proton spectra present in the space environment, with a 25 keV step, and total number of protons set to 1000. At each proton energy, simulations were conducted for 7 different thicknesses of the phase change layer, ranging from 50 nm to 200 nm with a 25 nm step.

After conducting these simulations, output files from TRIM, containing proton energy losses in the material, as well as structure dimensions and densities of the constituting materials, were used as input data for a MatLab code that calculated the proton absorbed dose (proton dose) in the entire PCM cell (D_{cell}), as well as in the phase change layer of the cell (D_{layer}).

Four SRIM files called RANGE.TXT, IONIZ.TXT, VACANCY.TXT, and PHONON.TXT were used for calculations of the proton dose. RANGE.TXT file contains the ion range distribution, where distribution units are (atoms per cm^3)/(atoms per cm^2). The file IONIZ.TXT provides the energy loss of ions to the target electrons, *i. e.* ionization loss rates in units eV/Å per ion (1Å = 10^{-10} m). The file VACANCY.TXT tabulates the energy loss to the target producing vacancies in unit vacancies/Å per ion, while the file PHONON.TXT provides the ion's energy loss to the target phonons in units eV/Å per ion. All four files give spatial information in units of Å. The text at the beginning (and end, in the case of VACANCY.TXT) of these files had been deleted prior use in MatLab code. From these four files, two columns of data were used: the first column representing ion depth

and the second representing ion distribution, ionization losses, vacancy or phonon production, depending on the file used. The proton dose in the whole PCM cell has been calculated according to the following equation

$$D_{\text{cell}} = \frac{e}{1000} a \sum_{i=1}^{6} \frac{1}{\rho_i} \sum_j f_j R_j (I_j + V_j + P_j) \quad (1)$$

whereas the proton dose in the active layer is determined as

$$D_{\text{layer}} = \frac{e}{1000} \frac{a}{\rho_4} \sum_j f_j R_j (I_j + V_j + P_j) \quad (2)$$

where, e is the elementary electric charge, a – the depth segment (in units cm), ρ_{i} – the density of layer i (in units g/cm^3), f_j – the ion fluence (in units ions per cm^2) in j-th segment. R_j – the ion distribution in segment j [in units (atoms per cm^3)/(atoms per cm^2)] and I_j, V_j, and P_j are energy losses due to ionization, vacancy productions, and phonons, respectively (in units eV/cm/ion). To obtain the energy loss due to vacancy production in appropriate units (eV/cm per ion), the data from the file VACANCY.TXT should be multiplied by the binding energy of the atom to its lattice site (in units eV per vacancy). Fluence in segment j is given by

$$f_j = f_{j-1} - R_{j-1} f_{j-1} a \quad (3)$$

for the values of j from 2 to 100, while f_1 is the ion fluence incident on the first layer.

RESULTS OF PROTON DOSE CALCULATIONS AND DISCUSSION

The results of calculations of the proton dose in phase change memory cells are shown in figs. 3-6.

Figure 3 shows the calculated value of the proton dose in the whole PCM cell vs. proton energy (E_{p}) for different thicknesses of the phase change layer. Figures 3(a)-(c) show the proton dose when the phase change material is GST, ASS, and SST, respectively. The lowest energy used in the simulations is 50 keV. When proton energy increases to 100 keV, the proton dose increases mildly. For energies higher than 200 keV, the proton dose drops rapidly. It can be noticed that for lower values of the phase change layer thickness, the maximum proton dose is obtained at low proton energies. For thicker phase change layers (175 nm and 200 nm), a plateau is visible, *i. e.* the maximum proton dose is obtained in a wide range of energies (100-150 keV). When GST is used for the active layer of the PCM cell, this plateau is widest and most obvious.

Maximum and minimum values of the proton dose in the entire PCM cell for the specified range of energies and thicknesses, for all three active layer materials, are given in tab. 1.

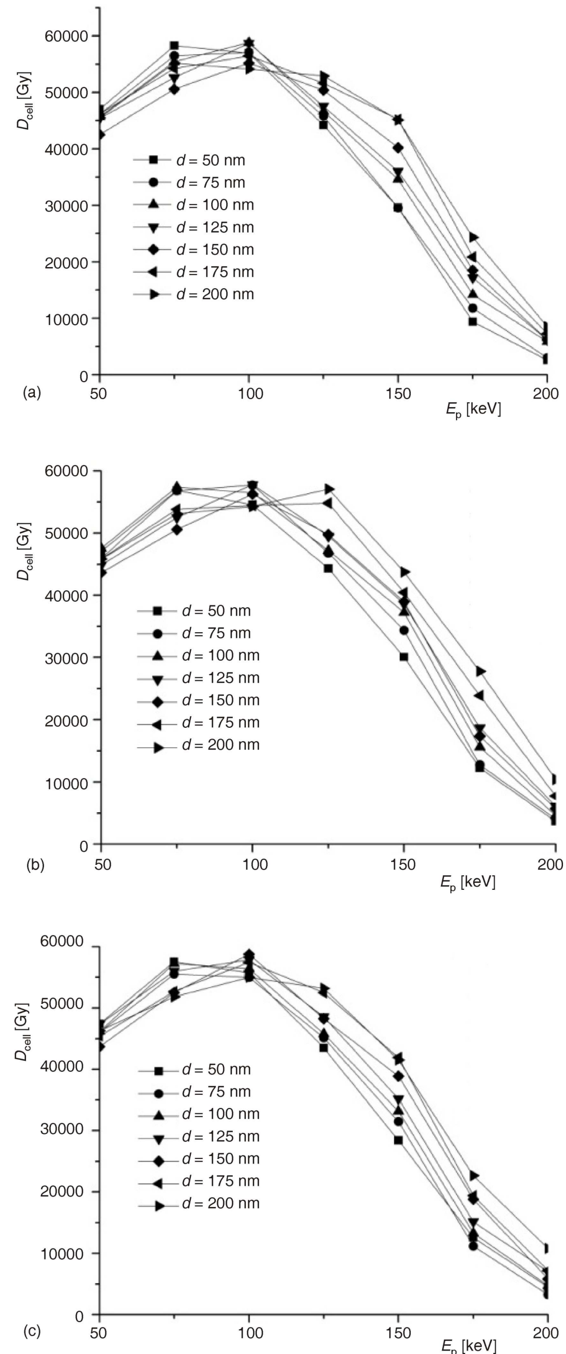

Figure 3. Proton dose in the whole PCM cell (D_{cell}) *vs.* proton energy (E_{p}) for different thicknesses of the phase change layer, where the material used for this active layer is (a) GST, (b) ASS, and (c) SST

Figure 4 presents the calculated values of the proton dose in the active layer of the PCM cell *vs.* proton energy (E_{p}) for different thicknesses of the phase change layer. Figures 4(a)-(c) show the proton dose when the phase change material is GST, ASS, and SST, respectively. As the graphs in fig. 4 show, D_{layer} peaks distinctly around 75-100 keV. The rise to this peak value at lower proton energies is steep, while the decline at higher proton energies is much more graduate. The maximum and minimum values of D_{layer} for

Table 1. Maximum and minimum values of the proton dose in the whole PCM cell and in the active layer, for the specified range of energies and thicknesses and for all three active layer materials

Phase change material	D_{cell} [Gy]		D_{layer} [Gy]	
	Maximum value	Minimum value	Maximum value	Minimum value
GST	58809 (100 keV, 100 nm)	2618.1 (200 keV, 50 nm)	25572 (100 keV, 200 nm)	0 (200 keV, 50 nm)
ASS	57826 (100 keV, 125 nm)	3651.1 (200 keV, 50 nm)	26328 (100 keV, 200 nm)	0 (200 keV, 50 nm)
SST	58765 (100 keV, 150 nm)	3273.1 (200 keV, 75 nm)	23884 (100 keV, 200 nm)	230.98 (200 keV, 75 nm)

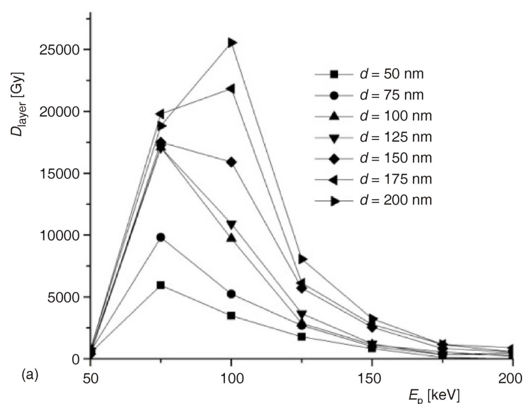

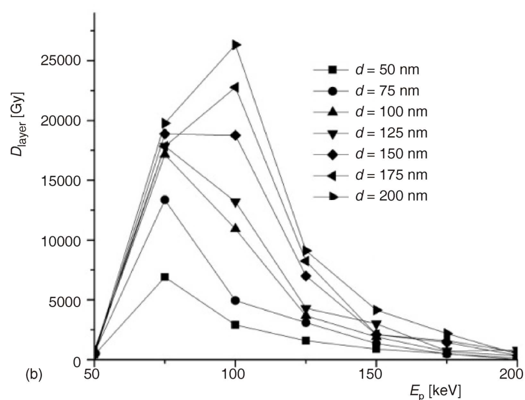

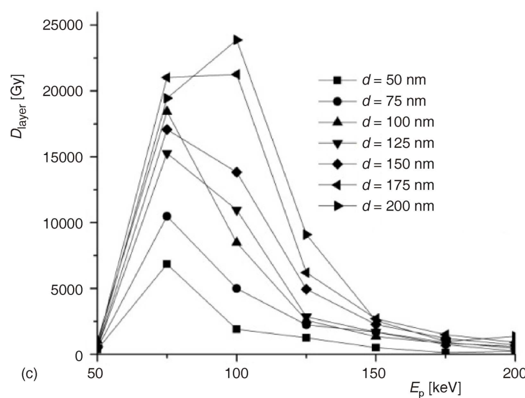

Figure 4. Proton dose in the active layer of the PCM cell (D_{layer}) *vs.* proton energy (E_p) for different thicknesses of the phase change layer, where the material used for this active layer is (a) GST, (b) ASS, and (c) SST

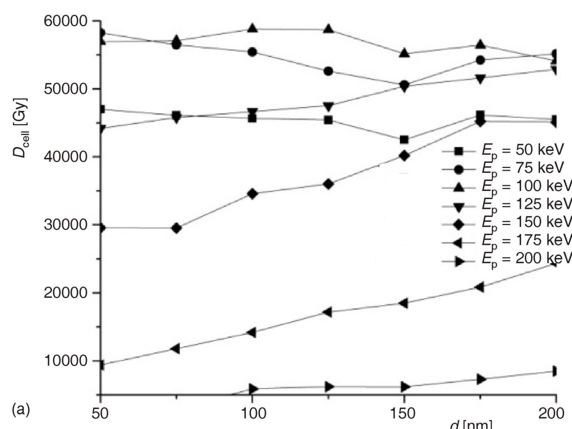

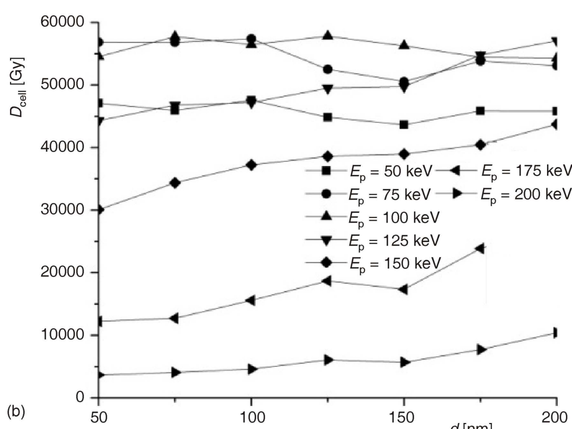

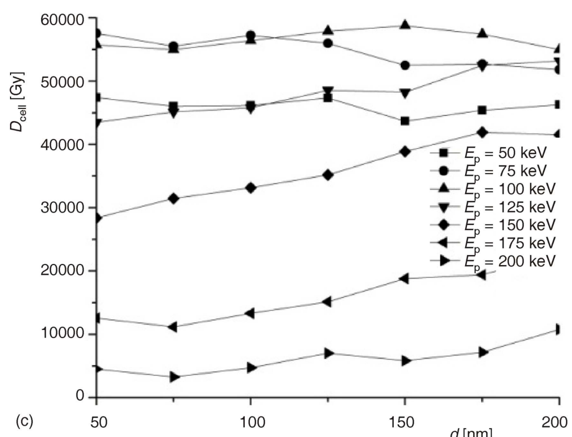

Figure 5. Proton dose in the whole PCM cell (D_{cell}) *vs.* the thicknesses of the phase change layer (*d*) for different proton energies, where the material used for the active layer is (a) GST, (b) ASS, and (c) SST

the specified range of energies and thicknesses for all three active layer materials are given in tab. 1, also.

Figure 5 presents the calculated value of the proton dose in the whole PCM cell (D_{cell}) *vs.* thicknesses of the phase change layer (*d*) for different proton energies. Figures 5(a)-(c) show the proton dose when the phase change material is GST, ASS, and SST, respectively.

In fig. 5 there are two distinct set of curves. The first set contains two curves representing D_{cell} depend-

ence on the active layer thickness for incident proton energies of 175 keV and 200 keV. For lower energies (50, 75, 100, and 125 keV), there is a second group of curves with values of D_{cell} that are several times higher.

For SST-based PCM cells and thicknesses higher than 100 nm, the maximum value of D_{cell} is obtained with 100 keV protons, while for thicknesses bellow this value, maximum D_{cell} is reached with 75 keV protons. The same relation applies to GST-based PCM cells, but with the threshold active layer thickness of 75 nm.

Figure 6 presents the calculated values of the proton dose in the active layer of the PCM cell (D_{layer}) *vs*. the thickness of the phase change layer (d) for different proton energies. Figures 6(a)-(c) show the proton dose when the phase change material is GST, ASS, and SST, respectively.

By inspecting figures shown below, it becomes clear that the relation between the D_{layer} and active layer thickness is nearly constant for energies of 50, 175 and 200 keV. For all three materials, there are two curves that stand apart from the rest, corresponding to proton energies of 75 and 100 keV. The D_{layer} for these proton energies is one or two orders of magnitude higher than for other proton energies used in the simulations. This implies that the PCM layer is most sensitive in the narrow range of energies between 75 and 100 keV. The lowest values of D_{layer} are found at proton energies of 50 keV and 200 keV.

Another important quantity to examine is the relative absorbed dose (D_{rel}), defined as the percentage ratio of D_{cell} to D_{layer}. Values for all three active layer materials are given in tabs. 2-4. Values of D_{rel} are in the range of 1% to over 40%. Maximum D_{layer}/D_{cell} ratios for all three material are obtained for proton energy of 100 keV and an active layer thickness of 200 nm.

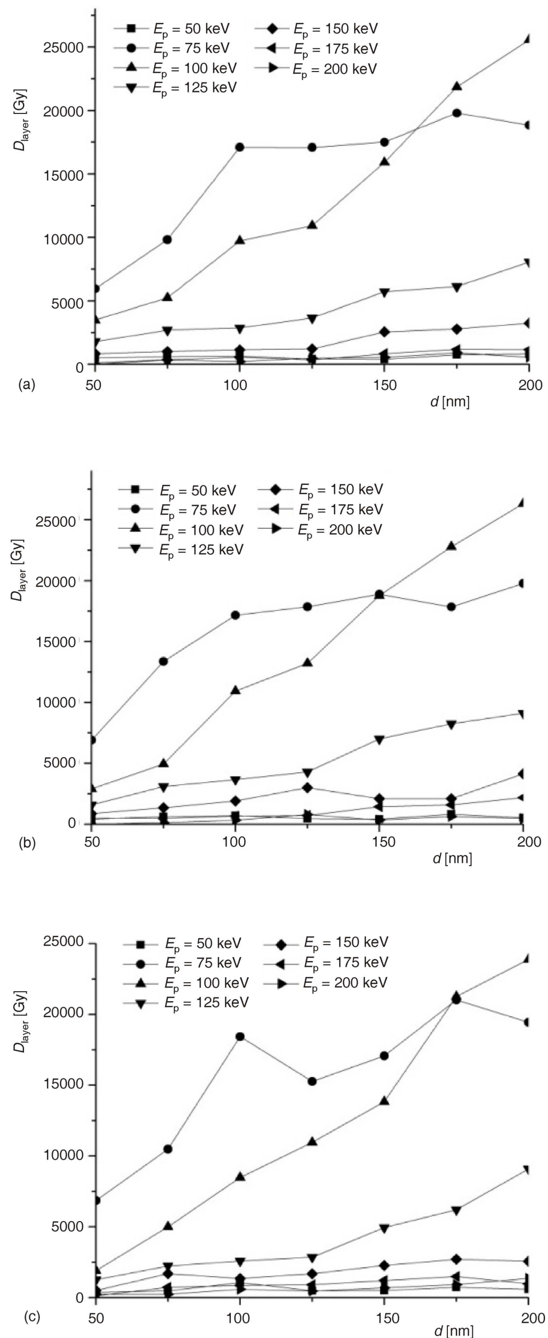

Figure 6. Proton dose in the active layer of the PCM cell (D_{layer}) *vs*. the thicknesses of the phase change layer (d) for different proton energies, where the material used for this active layer is (a) GST, (b) ASS, and (c) SST

ANALYSIS OF POSSIBLE RADIATION-INDUCED EFFECTS IN THE PCM CELL

Based on experimentally obtained radiation effects in different types of memories (EPROM and EEPROMs) [23, 24], the influence of radiation on

Table 2. Relative absorbed dose (D_{rel}) dependence on the thickness of the phase change layer (d) and proton energy (E_p), where the materials used for the active layer is GST

	D_{rel} [%]						
	50 keV	75 keV	100 keV	125 keV	150 keV	175 keV	200 keV
50 nm	1.0780	10.2200	6.1120	4.0247	2.8400	1.2725	0
75 nm	1.3535	17.3918	9.1823	5.8866	3.3657	2.9429	11.0398
100 nm	1.4540	30.8514	16.5325	6.1328	3.2940	4.0116	3.6627
125 nm	0.9440	32.4810	18.6045	7.6897	3.3748	2.0749	7.9205
150 nm	0.9017	34.6125	28.8450	11.3528	6.3620	4.5173	9.0820
175 nm	1.6488	36.4948	38.7138	11.8646	6.1323	5.5743	12.4180
200 nm	1.7879	34.1329	47.2374	15.2634	7.1853	4.7279	6.6502

Table 3. Relative absorbed dose (D_{rel}) dependence on the thickness of the phase change layer (d) and proton energy (E_p), where the materials used for the active layer is ASS

	D_{rel} [%]						
	50 keV	75 keV	100 keV	125 keV	150 keV	175 keV	200 keV
50 nm	0.8925	12.1635	5.3372	3.5938	2.9342	4.1074	0
75 nm	1.3767	23.5265	8.5653	6.6089	3.9527	3.7563	2.8055
100 nm	1.4938	29.8896	19.3694	7.7863	5.1388	4.3249	7.4172
125 nm	1.0163	33.9992	22.8602	8.6741	7.8063	3.8980	13.2756
150 nm	0.9640	37.3309	33.3407	14.0762	5.4220	8.3200	6.1249
175 nm	1.8179	33.1526	41.8403	15.0502	5.1947	6.6929	8.3798
200 nm	1.1847	37.2446	48.4735	15.9657	9.4824	7.8936	4.4915

Table 4. Relative absorbed dose (D_{rel}) dependence on the thickness of the phase change layer (d) and proton energy (E_p), where the materials used for the active layer is SST

	D_{rel} [%]						
	50 keV	75 keV	100 keV	125 keV	150 keV	175 keV	200 keV
50 nm	0.7944	11.9085	3.4007	2.8895	1.7779	0.9663	5.1519
75 nm	1.0376	18.8840	9.0905	4.9605	5.3562	6.6049	7.0572
100 nm	2.2828	32.1989	15.0377	5.6441	4.0583	6.379	12.3152
125 nm	1.0243	27.3154	18.9381	5.8681	4.7952	5.9838	6.6461
150 nm	1.1410	32.5274	23.5418	10.2426	5.8391	6.4457	12.0051
175 nm	1.6207	39.9038	37.0418	11.8207	6.4491	7.6638	12.7521
200 nm	1.2874	37.5340	43.4429	17.0891	6.1740	4.3161	12.6753

PCM cell's characteristics, functionality and hardness is analyzed in the following paragraphs.

The obtained results of the proton dose represent the contribution of three types of energy losses: ionization, phononic excitations of the crystal lattice, and atomic displacement.

The part of the proton dose that corresponds to phononic excitations manifests itself as thermal heating of the active layer material [25]. Special attention should be paid to ion energy losses to phonons in PCM cells due to its unique way of functioning based on phase transition. Temperatures that lead to phase transitions, *i. e.* transition temperatures (T_t) in GST, SST, and ASS materials, are in the range from 100 °C to 300 °C [14, 26, 27]. Based on these transition temperatures, activation energies which lead to phase transitions are assessed as $E_a = k_B T_t$, where k_B is the Boltzmann constant and T_t is the transition temperature. The assessed value of E_a is of the order of 10^{-21} J. Values of energy transferred from protons to phonons (E_{phon}) were extracted from the outputs of the performed simulations, in the critical proton energy range (75-100 keV), and found to be of the order of 10^{-15} J. It is obvious that $E_{phon} \gg E_a$, which implies that the heating of the active material induced by a proton beam may change its phase, *i. e.* the logic state of the PCM cell could be perturbed. RESET to SET transitions are less likely to be induced in irradiated PCM cells, due to the inherent immunity of the amorphous phase to radiation effects, while radiation-induced SET to RESET transitions have actually been observed in experiments [28].

Another possible scenario for radiation-induced changes in a PCM cell involves the accumulation of atomic displacements in the active layer material. Radiation could cause the crystalline-to-amorphous phase change by creating a large number of atomic displacements which disrupt the highly ordered lattice structure of the crystalline phase [25]. Results of proton transport simulations have shown that the largest number of displacements occur in ASS, at a proton energy of 75 keV and active layer thickness of 100 nm.

Single event effects in phase change memories have previously been investigated in [29]. The absorbed dose from highest-LET ions used in that paper (Xe), at fluences applied therein, has been estimated at ~10^2 Gy, while in our investigations the calculated doses in the phase change material were in the 10^2-10^4 Gy range. Although the results in [29] suggest that PCM cells are insensitive to heavy-ion strikes, they could be prone to effects of higher absorbed doses that we have obtained. Our calculations indicate that certain realistic fluence values of low energy protons can deposit these high doses in PCM cells, either over a long time period or in high dose-rate irradiation conditions.

Even if radiation-induced changes alone are not able to initiate a phase change from the crystalline to the amorphous state, when superimposed with thermally generated Frenkel pairs and other random defects present in the crystal, they could push the cell state beyond a margin level into an undefined logic state, corresponding to the active material being in a glassy phase, between the polycrystalline and amorphous ones.

Thermal annealing of irradiated materials is commonly performed by substantially heating and gradually cooling the material, whereby radiation produced defects recombine. In the PCM cell, thermal annealing could be achieved by a modified SET operation. In case of an irregular state of the memory cell, *i. e.* when the cell is in-between crystalline and amorphous phases, the cell state could be unambiguously defined by introducing an additional SET pulse, which would bring the memory cell to a well defined SET state. After this procedure, however, the logic state of the memory cell would be "1", regardless of its previous state, *i. e.* the stored data would be lost.

CONCLUSIONS

Simulations of proton interactions with the PCM cell were conducted. Values of proton energy loss were used to calculate the proton absorbed dose in the entire cell and in the phase change layer alone. The values obtained for the absorbed dose in investigated PCM cells are of the order of magnitude of 10^4 Gy which is in compliance with the reported results of proton dose assessment in similar nanometer memory cell structures [8]. Three most commonly used phase change materials were investigated. The results of these simulation-based calculations of the proton dose suggest that the investigated phase change materials are most sensitive within the narrow range of proton energies between 75 and 100 keV. With an increase in the thickness of phase change material, the proton dose in the whole PCM cell remains nearly constant, while the active layer dose increases significantly in the crytical proton energy range (75-100 keV). The exposure of PCM cells to proton beams could influence the device's operation in several ways: thermal heating of the active material and accumulation of atom displacements which, in synergy with other possible defects in the cell, could affect the stability of the PCM cell. The annealing of a PCM cell brought to an undefined logic state by irradiation can be accomplished by introducing a modified SET pulse, at the expense of losing previously stored data and slowing down memory operation.

This type of calculations allow the assessment of the proton dose and the overview of radiation effects in the active layer of the PCM cell and the PCM cell itself for proton fluences that represent real radiation environment, whereas actual experiments cannot separate the influence of radiation on the PCM cell alone, without including the effects on peripheral circuits.

ACKNOWLEDGEMENT

The Ministry of Education, Science and Technological Development of the Republic of Serbia supported this work under contract 171007.

AUTHOR CONTRIBUTIONS

Theoretical analysis carried out by N. Zdjelarević and M. Lj. Vujisić. Simulations and calculations were carried out by N. S. Zdjelarević. All authors analysed and discussed the results. The manuscript was written by N. S. Zdjelarević and M. Lj. Vujisić, and the figures were prepared by N. S. Zdjelarević.

REFERENCES

[1] Ovshinsky, S., Reversible Electrical Switching Phenomena in Disordered Structures, *Physical Rev. Lett., 21* (1968), 20, pp. 1450-1453

[2] Neale, R. G, *et al*., First Ovonic Memory, *Electronics, 43* (1970), 1, pp. 56-60

[3] Wang, K., *et al*., Emerging Memory Devices, *Circuits and Devices Magazine, 22* (2006) 3, pp. 12-21

[4] Muller, G., *et al*., Status and Outlook of Emerging Nonvolatile Memory Technologies, Electron Devices Meeting, 2004, IEDM Technical Digest, IEEE, 2004, pp. 567-570

[5] Kinam, K., Lee, S. Y., Memory Technology in the Future, *Microelectronic Engineering, 84* (2007), 9-10, pp. 1976-1981

[6] Barth, J. L., *et al*., Space, Atmospheric, and Terrestrial Radiation Environments, *IEEE Transactions on Nuclear Science, 50* (2003), 3, pp. 466-482

[7] Ferreira, A. P., *et al*., Using PCM in Next-Generation Embedded Space Applications, 16th Real-Time and Embedded Technology and Applications Symposium, IEEE, 2010, pp. 153-162

[8] Knežević, I., *et al*., Absorbed Dose Assessment in Particle-Beam Irradiated Metal-Oxide and Metal-Nonmetal Memristors, *Nucl Technol Radiat, 27* (2012), 3, pp. 290-296

[9] Vujisić, M., *et al*., Simulated Radiation Effects in the Superinsulating Phase of Titanium Nitride Films, *Nucl Technol Radiat, 26* (2011), 3, pp. 256-260

[10] Vujisić, M., *et al*., Simulated Effects of Proton and Ion Beam Irradiation on Titanium Dioxide Memristors, *IEEE Transactions on Nuclear Science, 57* (2010), 4, pp. 1798-1804

[11] Siegel, J., *et al*., Rewritable Phase-Change Optical Recording in $Ge_2Sb_2Te_5$ Films Induced by Picosecond Laser Pulses, *Applied Physics Letters., 84* (2004), 13, pp. 2250-2252

[12] Senkader, S., *et al*., Models for Phase Change of in Optical and Electrical Memory Devices, *Japanesse Applied Physics, 95* (2004), 2, pp. 504-511

[13] Wang, K., *et al*., Assessment of Se Based Phase Change Alloy as a Candidate for Non-Volatile Electronic Memory Applications, *Applied Physics A, 81* (2005), 8, pp. 1601-1605

[14] Wang, K., *et al*., Phase Change Properties of Ternary $AgSbSe_2$ Chalcogenide Films, *Journal of Ovonic Researh, 2* (2009) 4, pp. 61-65

[15] Zhang, T., *et al*., Investigation of Phase Change $Si_2Sb_2Te_5$ Material and its Application in Chalcogenide Random Access Memory, *Solid-State Electronics, 51* (2007), 6, pp. 950-954

[16] SangBum, K., Scalability and Reliability of Phase Change Memory, Ph. D. dissertation of Department of Electrical Engineering, Stanford University, USA, 2012, pp. 12-16

[17] Wong, P., *et al.*, Phase Change Memory, *Proceedings of the IEEE*, *98* (2012), 2, pp. 2201-2227
[18] Wuttig, M., Yamada, N., Phase-Change Materials for Rewriteable Data Storage, *Nature Materials, 6* (2007), 12, pp. 824-1004
[19] Qu, L. W., *et al.*, SET/RESET Properties Dependence of Phase-Change Memory Cell on Thickness of Phase-Shange Layer, *Solid-State Electronics 56* (2011), 1, pp. 191-195
[20] Tsoulfanidis, N., Energy Loss and Peneration of Radiation through Matter, Chapter 4, in: *Measurement and Detection of Radiation*, 2nd ed., Taylor & Francis, Washington DC, USA, 1995
[21] Ziegler, J. F., *et al.*, SRIM (The Stopping and Range of Ions in Matter), Available on line :http://www.srim.org
[22] Timotijević, Lj., *et al.*, Simulation of Proton Beam Effects in Thin Insulating Films, *International Journal of Photoenergy*, *2013* (2013), 1, pp. 1-6
[23] Vujisić, M., *et al*., Comparison of Gamma Ray Effects on EPROM and E2PROM, *Nucl Technol Radiat, 27* (2009), 1, pp. 61-67
[24] Vujisić, M., *et al*., Radiation Hardness of COTS EPROMs and EEPROM, *Radiation Effects and Defects in Solids: Incorporating Plasma Science and Plasma Technology, 165* (2010), 5, pp. 362-369
[25] Was, G. S., Phase Stability under Irradiation, Chapter 9.7 in: *Fundamentals of Radiation Materials Science*, Springer, Berlin, 2007
[26] Zhang, T., *et al*., Investigation of Electron Beam Induced Phase Change in $Si_2Sb_2Te_5$ Material, *Applied Physics A, 90* (2008), 3, pp. 451-455
[27] Friedrich, I., *et al*., Structural Transformations of $Ge_2Sb_2Te_5$ Films Studied by Electrical Resistance Measurements, *Journal of Applied Physics, 87* (2000), 9, pp. 4130-4133
[28] Maimon, J., *et al*., Chalcogenide Memory Arrays: Characterization and Radiation Effects, *IEEE Transactions on Nuclear Science, 50* (2003), 6, pp. 1878-1884
[29] Gerardin, S., *et al*., Single Event Effects in 90 nm Phase Change Memories, *IEEE Transactions on Nuclear Science, 58* (2011), 6, pp. 2755-2760

Received on January 18, 2103
Accepted on September 12, 2013

**Невена С. ЗДЈЕЛАРЕВИЋ, Иван Д. КНЕЖЕВИЋ,
Милош Љ. ВУЈИСИЋ, Љубинко Ђ. ТИМОТИЈЕВИЋ**

ПРОРАЧУН ПРОТОНСКЕ ДОЗЕ У МЕМОРИЈСКИМ ЋЕЛИЈАМА СА ФАЗНО ПРОМЕНЉИВИМ СЛОЈЕМ ЗАСНОВАН НА СИМУЛАЦИЈИ

У раду се одређује протонска доза у целој меморијској ћелији са фазно променљивим активним слојем, као и у самом активном слоју ћелије, коришћењем Монте Карло симулација транспорта протона. Модел меморије састоји се од активног слоја који је смештен између две TiW електроде и два $ZnS-SiO_2$ изолаторска филма. Коришћени фазно променљиви материјали су: Ge_2Sb_2Te (GST), $AgSbSe_2$ (ASS) и $Si_2Sb_2Te_5$ (SST). Проучавани су ефекти излагања ових меморија различитих дебљина протонима различитих енергија. Приказане су промене изазване проласком протона у испитиваним меморијама, укључујући акумулацију измештених атома и термално загревање активног слоја. Разматрани су могући ефекти ових промена на функционисање меморијских ћелија.

Кључне речи: меморијске ћелије са фазно променљивим слојем, фазно променљиви материјал, излагање протонским сноповима, Монте Карло метода, апсорбована доза